Size and temperature dependence of electrical resistance and thermoelectric power of Bi2Te2Se1 thin films

V. Damodara Das and S. Selvaraj

Citation: J. Appl. Phys. **83**, 3696 (1998); doi: 10.1063/1.366594
View online: http://dx.doi.org/10.1063/1.366594
View Table of Contents: http://jap.aip.org/resource/1/JAPIAU/v83/i7
Published by the American Institute of Physics.

Size and temperature dependence of electrical resistance and thermoelectric power of $Bi_2Te_2Se_1$ thin films

V. Damodara Das[a] and S. Selvaraj
Thin Film Laboratory, Department of Physics, Indian Institute of Technology, Madras, Chennai 600 036, India

(Received 7 July 1997; accepted for publication 10 December 1997)

Thin films of $Bi_2Te_2Se_1$ of various thicknesses have been deposited on clean glass plates using the flash evaporation technique. Electrical resistance and thermoelectric power measurements have been carried out on these films in the temperature range 300–485 K. The thickness dependences of electrical resistivity and thermoelectric power of the films have been analyzed using the effective mean-free path model. The thickness dependence of activation energy of the films is explained by Seto's polycrystalline model. Various material parameters such as mean-free path and Fermi energy have been calculated from the analysis of experimental data. The thermoelectric power factor of the films has been calculated using the measured electrical resistivity and thermoelectric power values. © *1998 American Institute of Physics.* [S0021-8979(98)10006-3]

I. INTRODUCTION

The thermoelectric effect was exploited for temperature measurements and power generation right from its discovery. Nevertheless, there was no vigorous research on thermoelectrics until the 1950s when Ioffe[1] suggested that the solid solutions of isomorphic compounds can exhibit increased thermoelectric efficiency. He suggested that thermoelectric refrigeration could be accomplished with the best thermoelectric materials. It was found that solid solutions based on Bi_2Te_3 are good thermoelectric materials around room temperature. Based on this idea there has been a lot of research on $Bi_2Te_{3-x}Se_x$ materials in the bulk state regarding their transport and structural properties.[2–9] But only very little work has been carried out on these materials in the thin film state regarding thermoelectric properties.[10,11] Scientists have concluded that thermoelectric modules using thin films give relatively higher voltage for power generation than the bulk thermoelectric modules. Thus, research into the physical properties of thin films of thermoelectrically important $Bi_2Te_{3-x}Se_x$ materials is very essential. It was suggested in Refs. 10 and 11 that flash evaporation of these materials gives stoichiometric and homogeneous films. Il-Hd-Kim *et al.*[12–14] have fabricated a Bi–Sb–Te–Se thin film power generator and have investigated its performance. Wagner *et al.*[15,16] have produced multilayer thermoelectric films and devices by the sputtering technique and have tested these films. They have deposited multilayer films of $(Bi_{1-x}Sb_x)_2(Te_{1-y}Se_y)_3$ alloy by magnetron sputtering[17] and have shown that no interdiffusion takes place at high deposition temperatures and that there is no degradation of thermoelectric properties of the structures. They have also suggested that the thermoelectric figure of merit of these structures can be enhanced by optimizing the composition of the barrier in the structure. Efforts were made to test the quantum well concept for $Bi_{0.9}Sb_{0.1}$ and $PbTe_{0.8}Se_{0.2}$ multilayer structures in Ref. 18 and new techniques were developed to pick out the relevant parameters which influence the thermoelectric properties of the structure. Farmer *et al.*[19–22] also fabricated multilayer thermoelectric films by sputter deposition and have evaluated these films as two-dimensional quantum-well structures.

Bi_2Te_3 and Bi_2Se_3 form continuous series of solid solutions at temperatures above 500 °C.[23] This alloy crystallizes with a hexagonal structure and belongs to the space group $R\bar{3}m$.[5] The atomic arrangement is similar to Bi_2Te_3 in which the layers repeat the unit $Te^{(1)}$–Bi–$Te^{(2)}$–Bi–$Te^{(1)}$. In this article, we present the results of thermoelectric properties investigated and the physical parameters evaluated from the thermoelectric measurements of $Bi_2Te_2Se_1$ thin films prepared by the flash evaporation technique.

II. EXPERIMENT

Alloy of $Bi_2Te_2Se_1$ material was prepared under vacuum by melting the mixture of required amounts of 5*N* pure elements Bi, Te, and Se in a quartz ampoule. Each element was kept melted for 24 h and then the temperature of the furnace was maintained just above the liquidus temperature of the alloy for 48 h. The ampoule was shaken frequently to get the homogeneous melt. Then, the temperature was reduced to just below the liquidus temperature (630 °C) so that the alloy solidified after which it was annealed at this temperature for four days. Then the alloy was gradually brought to room temperature. The alloy formation was confirmed by x-ray diffraction analysis (XRD). The alloy thus prepared was powdered into fine particles and was used for preparing thin films by the flash evaporation technique. The substrates (glass plates with lateral dimensions 2.5 cm×7.5 cm) were cleaned in the following way. The glass plates were kept immersed in dilute chromic acid for 48 h. They were later put in an ultrasonic vibrator along with soap water and cleaned for half an hour. Finally they were cleaned with de-ionized water and then dried. The glass plates cleaned in

[a]Electronic mail: vddas@acer.iitm.ernet.in

this way were used for the deposition of the films. Thin films of various thicknesses were deposited in a vacuum of 2×10^{-5} Torr. The thickness and the deposition rate were monitored using a quartz crystal monitor. The same physical configuration was maintained during each deposition of the films. XRD and transmission electron microscopy (TEM) analyses were used for the structural characterization of the films. The compositional analysis was made by the energy dispersive analysis of x-rays (EDAX).

The thermoelectric power was measured for these thin films in the temperature range 300–485 K using the integral technique. One end of the film was heated and the other end was kept at a constant temperature, in this case, room temperature. The electrical resistance of these films in the temperature range 300 K–485 K was measured. Large-area copper pad pressure contacts were used for all the measurements. Two separate films, one for measuring thermoelectric power and an another for measuring electrical resistance, were used. Both these films were grown simultaneously so that they had similar microstructures. Both the measurements were made using Keithley digital multimeters (model 196) which were automated using a computer. The details of automation are given elsewhere.[24] The temperature was measured using a copper-constantan thermocouple.

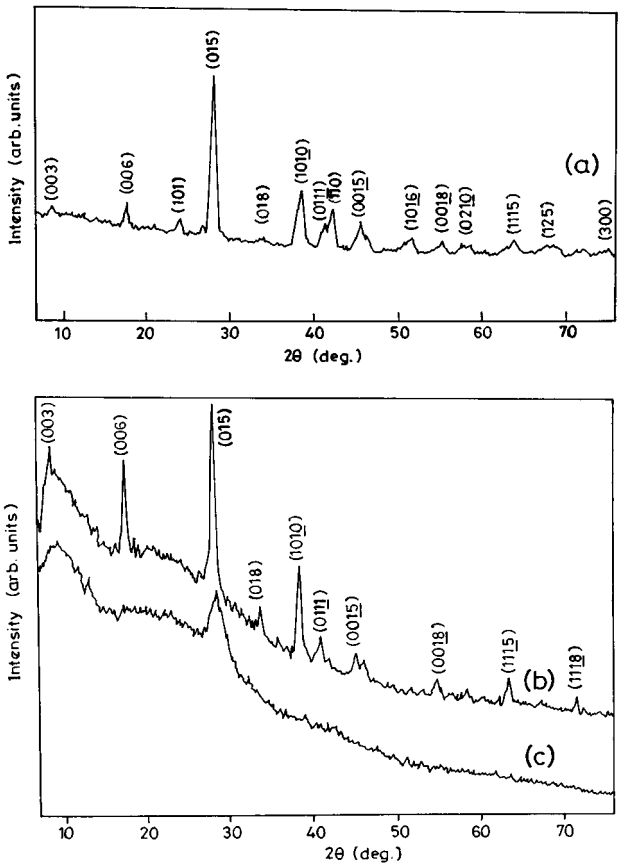

FIG. 1. X-ray diffractogram of $Bi_2Te_2Se_1$ alloy (a) bulk (b) annealed film (c) unannealed film, film thickness = 2000 Å.

TABLE I. Comparison of observed d values of bulk and thin films from XRD and electron diffraction data with ASTM standard d values of Bi_2Te_3 (set 15 863) and Bi_2Se_3 (set 12 732) materials.

ASTM d values Å			d values observed Å		
			XRD	thin film	
Bi_2Te_3	Bi_2Se_3	hkl	bulk	XRD	SAD
10.16		003	10.161	10.046	
5.078	4.80	006	5.038	5.034	
3.767	3.56	101	3.677		3.66
3.222	3.03	015	3.142	3.154	3.10
2.689	2.54	018	2.636	2.646	
2.376	2.23	$10\bar{1}0$	2.323	2.332	2.17
2.238	2.10	$01\bar{1}1$	2.180	2.193	
2.192	2.07	$1\bar{1}0$	2.133		
2.031	1.907	$00\bar{1}5$	1.990	1.996	1.98
2.013		$1\bar{1}6$		1.964	
1.702		$10\bar{1}6$	1.770		
1.693		$00\bar{1}8$	1.664	1.664	
1.611	1.519	$02\bar{1}0$	1.600		
1.490	1.404	$11\bar{1}5$	1.454	1.461	1.47
1.397	1.320	$12\bar{5}$	1.383		1.39
1.340		$11\bar{1}8$		1.314	
1.266		$30\bar{0}$	1.263		

III. RESULTS AND DISCUSSION

A. Structural analysis

Structural analyses using XRD and TEM showed the polycrystalline nature of the films with hexagonal structure. Figure 1 shows the x-ray diffraction pattern of the bulk, annealed and unannealed thin films. The d values obtained from the x-ray diffraction patterns have been compared with the American Society for Testing and Materials (ASTM) d values of Bi_2Te_3 and Bi_2Se_3 alloys in Table I: The lattice parameters were found to be $a = 4.27$ Å, and $c = 30.23$ Å. Thus, the thin films have the same structure as that of the bulk alloy which is analogous to that of Bi_2Te_3 and Bi_2Se_3 alloys. The grain size of the films was calculated from the x-ray diffraction pattern using the Debye–Scherrer formula,[25] $L = 0.9\lambda/B \cos\theta$, where L is the grain size of the films, λ the wavelength, B the full width at half maximum, and θ the diffraction angle. It is found that the grain size of the film increases with increasing thickness (Table II). The TEM micrograph and the corresponding selected area diffraction (SAD) pattern for a film of thickness 1250 Å are shown in Fig. 2. The compositional analysis of the films by EDAX analysis indicates that there is a loss of tellurium in the annealed films (see Table III). This evaporation occurs in thin films because atomic bonds are not equivalent in all the directions at the surface. Even though selenium is more vola-

TABLE II. Variation of grain size and activation energy with thickness.

Thickness Å	Grain size Å	Activation energy (meV)
900	144	54
1150	200	46
1250	205	43
2000	190	43
3000	215	32

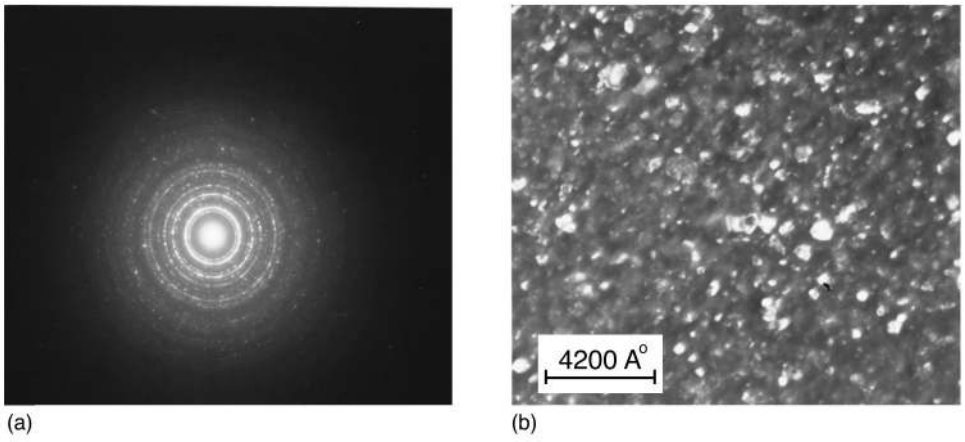

FIG. 2. (a) SAD pattern and (b) electron micrograph of thin film of thickness 1250 Å.

tile than tellurium, it is tellurium which gets evaporated easily from the material. This is because selenium, being more electronegative than tellurium, goes to the $Te^{(2)}$ site in the $Te^{(1)}$–Bi–$Te^{(2)}$–Bi–$Te^{(1)}$ layer of Bi_2Te_3 and so the binding energy of Se is more than Te.

B. Electrical resistance and its temperature dependence

Electrical resistance measurements were made on these as-grown films in the temperature range 300–485 K. It is observed that the resistance during the cooling cycle is always lower than that during the heating cycle for the films (Fig. 3). This is because of the fact that during the heating cycle all the frozen-in defects which are incorporated during the growth of the film are removed, reducing the number of defects, and hence, the number of scattering centers. But, for annealed films the resistance during the cooling cycle closely coincides with that in the heating cycle. Hence, for all our calculations we have used the data of the annealed films during the cooling cycle. The thermal activation energy of the films was determined from the slopes of $\mathrm{Ln}(R)$ versus $1000/T$ plots (Fig. 4) which were nearly linear. The values of activation energy are given in Table II. The linear plot also indicates the semiconducting behavior of the films. It is found that the activation energy is thickness dependent. Even though there is no systematic variation of activation energy with thickness, there is a general trend of decrease in activation energy with increase in thickness.

This can be explained to be due to the polycrystalline nature of the films as explained by Seto's[26] model. A polycrystalline film material contains a large number of microcrystallites with grain boundaries between them. At the grain boundary of each of the crystallites the incomplete atomic bondings can act as trap centers. These trap centers can trap the charge carriers at the grain boundaries, and hence, a space charge can be built up locally. This space charge depletes the region locally and also impedes the transit of the charge carriers from one crystallite to the other. Thus, at the grain boundary, the charge carriers see a barrier which affects the transport properties. Taking these effects into account, Seto derived an expression for the activation energy namely,

$$V_B = \frac{qL^2N}{8\epsilon}, \quad \text{for } LN < Q_t \tag{1}$$

$$V_B = \frac{qQ_t^2}{8\epsilon N}, \quad \text{for } LN > Q_t \tag{2}$$

where q is the electronic charge, L the grain size, N the density of dopent concentration, Q_t the density of surface states, and ϵ the dielectric permittivity.

TABLE III. Composition analysis through EDAX.

Elements	Compositions observed: Unannealed at. %	Compositions observed: Annealed at. %	Expected at. %
Bi	38.5	39.7	40
Te	43.1	37.3	40
Se	18.4	23.0	20

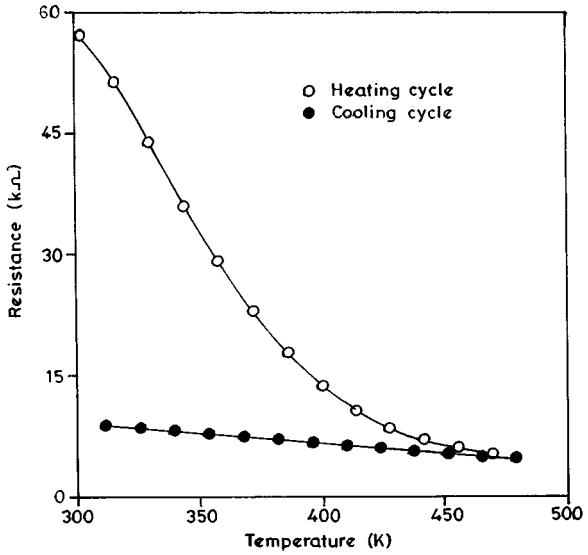

FIG. 3. Variation of resistance with temperature of a typical thin film during heating and cooling cycle.

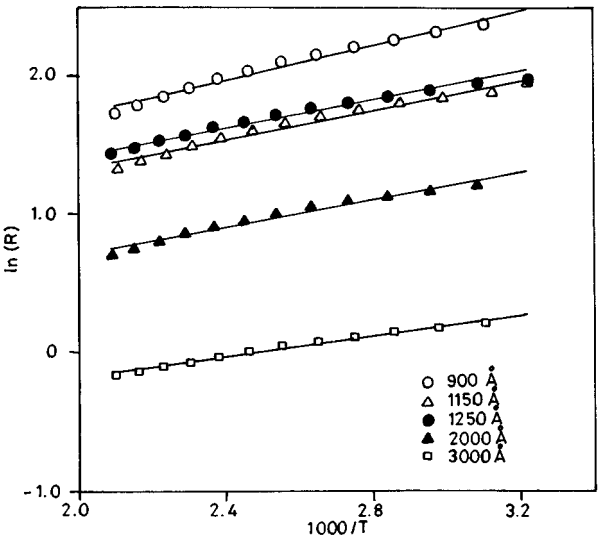

FIG. 4. Plot of Ln(R) vs 1000/T for different films.

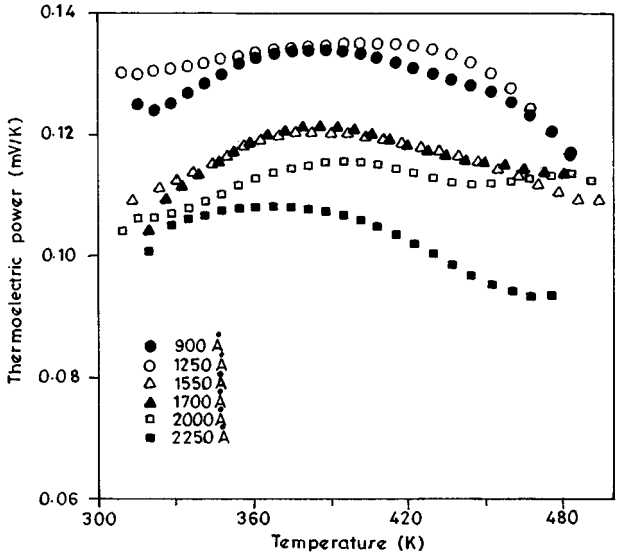

FIG. 5. Variation of thermoelectric power with temperature for thin films of different thicknesses.

The first equation suggests that as the grain size increases, the barrier height increases. But we observe that as the thickness (and hence, grain size) increases the activation energy decreases. Thus, the first condition can be ruled out and the second equation can be taken as the appropriate one. This indicates that the dopent concentration increases with thickness. This is supported by the fact that as the thickness increases, the resistivity decreases. Thus, the barrier height can decrease with increase in thickness. This type of behavior has been observed by Damodara Das *et al.* in $(Bi_{0.6}Sb_{0.4})_2Te_3$[27] and $Pb_{0.5}Sn_{0.5}Te$[28] thin films also. Also it is seen from the plot of Ln(R) versus 1000/T (Fig. 4) that in the case of low thickness films the experimental points slightly deviate from the straight line, whereas in the case of higher thickness films the points fit very well to a straight line. Actually, there are two contributions to the resistance of the films; one is from the bulk of the crystallites and the other is from the grain boundary region. The grain boundary affects the mobility of the charge carriers and Seto's model says that the mobility of the charge carriers depends exponentially on temperature. It is this effect on the mobility of the charge carriers which causes the deviation of the experimental points from the straight line in the case of low thickness films. As the thickness increases, the barrier height at the grain boundary decreases, and hence, the effect on mobility also decreases gradually. This is why the data points fit well to a straight line for higher thickness films.

C. Thermoelectric power

Thermal emf measurements on these films indicate their n-type conduction behavior. As shown in Fig. 5, there is a general trend of decrease in thermoelectric power with increase in thickness, as expected. It is known that the thermoelectric power of amorphous or disordered materials is high. Here, as the thickness increases, the grain size of the films increases, and hence, the extent of single crystallinity and orderliness also increases with thickness. So, the above result is expected. The thermoelectric power of the films was calculated from the measured thermal emf values by the least squares error analysis using spline functions. It is seen from the plot of thermoelectric power versus temperature (Fig. 5) that the thermoelectric power of the films initially increases with temperature showing the degenerate nature and then decreases with temperature after reaching a maximum. This is explained to be due to the following reasons:

The partial evaporation of Te atoms from the films, as evidenced from the EDAX analysis, produces vacancies in the films. These Te vacancies can be occupied by either Bi atoms or Se atoms. But, since Bi and Te have similar electronegativity and atomic radius, Bi atoms prefer to occupy tellurium sites as substitutes. This leads to the generation of acceptors and contributes to p-type charge carriers. Alternatively, Se atoms occupying the Te sites, leads to n-type charge carriers. In addition to the substitutional occupancy of Te sites by Bi/Se atoms, these atoms sometimes also occupy the interstitial positions. This also can lead to n- or p-type charge carriers depending upon the type of atoms—(Bi) or (Se). Thus, in effect there are two types of charge carriers in the films. Hence, the transport properties of the films have to be explained by a two carrier model even though n-type carriers are the majority carriers. The thermoelectric power of a two carrier type material is given by the expression,[29]

$$S = -(k/e)\,\frac{n\mu_n(2-\epsilon/kT) - p\mu_p(2-\xi/kT)}{n\mu_n + p\mu_p}, \tag{3}$$

where $n(p)$ is the electron (hole) concentration, $\mu_n(\mu_p)$ the electron (hole) mobility, ϵ the chemical potential for electrons and ξ the chemical potential for holes.

This equation suggests that the product of mobility and carrier concentration determines the sign of thermoelectric power. It has been reported[30] that in these materials the mobility of the electrons varies as T^{-2} at high temperatures continuously. Thus, the decrease of thermoelectric power after reaching a maximum, can be attributed to the decrease of the mobility of the electrons. But, as temperature increases,

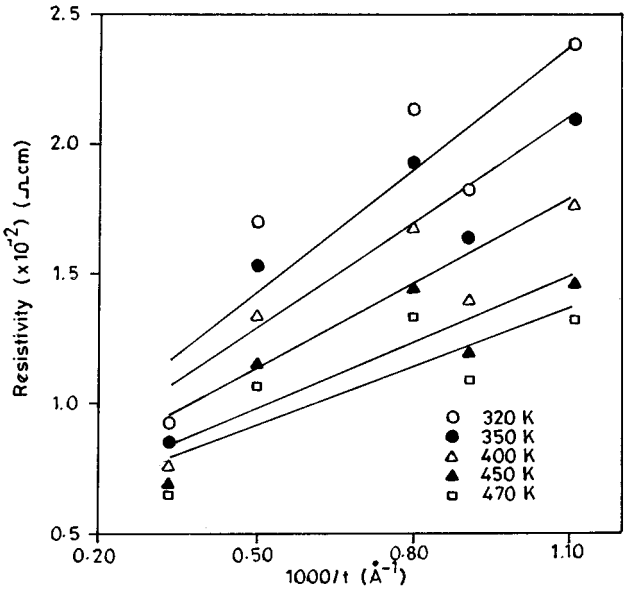

FIG. 6. Plot of resistivity vs reciprocal thickness at different temperatures.

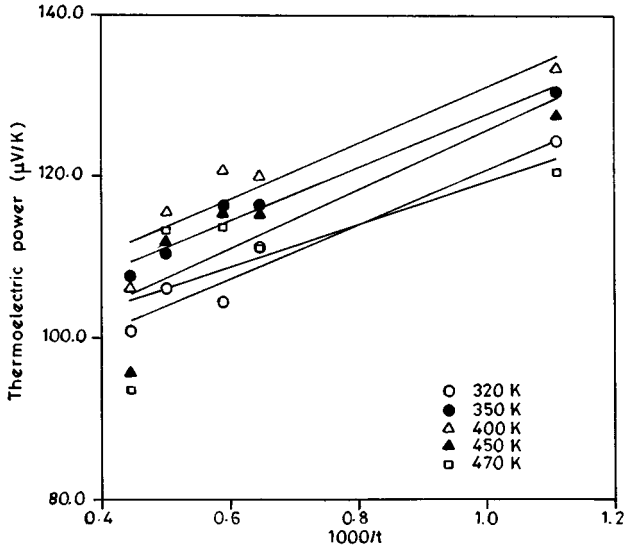

FIG. 7. Plot of thermoelectric power vs reciprocal thickness at different temperatures.

we may expect a sign change at a still higher temperature. On the other hand, thermoelectric power starts to increase once again at a temperature around 450 K. This is clearly revealed in the higher thickness films. This can be explained as follows.

Generally, it is observed that when these films are exposed to the atmosphere, oxygen adsorption takes place on their surface. This is indicated by the increase of the resistance of the films as a function of time. Similarly, a decrease of resistance of the films is observed while evacuating the air, which indicates that the adsorbed oxygen atoms are getting desorbed. But, as the resistance variation is only partially reversible, not all oxygen atoms are liberated. Thus, during heating the remaining oxygen atoms can be desorbed from the films at higher temperatures. This may lead to the creation of structural defects at higher temperatures releasing the bound electrons. This leads to an increase in the electron concentration, and hence, an increase in the thermoelectric power.

D. Thickness dependence of electrical resistivity and thermoelectric power—combined analysis

To account for the size effect on the transport properties, a number of theories[31–35] have been suggested. Tellier[36] was successful in getting a simplified analytical expression for electrical resistivity as a function of thickness namely,

$$\rho_f = \rho_g \left[1 - \frac{3(1-p) l_g}{8t} \right], \tag{4}$$

where ρ_g and l_g are, respectively, resistivity and mean-free path in the hypothetical bulk and p is the specularity parameter. The specularity parameter gives the fraction of the charge carriers which are specularly scattered at the surface. The above expression indicates that the values of ρ_g and l_g can be obtained from a plot of ρ_f versus reciprocal thickness. In this analysis, it is assumed that the carriers are all diffusely scattered and hence, p is assumed to be zero. Figure 6 shows a plot of ρ_f versus $1000/t$ with a straight line fit. The experimental points are a bit scattered because of experimental limitations. The values of ρ_g and l_g obtained are given in Table IV. It is seen that the mean-free path of the carriers decreases with temperature, as expected. The variation of ρ_g with temperature indicates the semiconducting behavior. The high value of ρ_g (resistivity of infinitely thick samples) is due to the microstructure; the sample contains very small grains with a large number of grain boundaries which impede the conduction of carriers as explained in Seto's model.

The size effect on thermoelectric power can give important physical parameters. According to the effective mean-free path model[37] which takes into account the grain bound-

TABLE IV. Variation of various physical parameters obtained through combined analysis of resistivity and thermoelectric power.

Temperature K	$\rho_g \times 10^{-3}$ Ω cm	S_g μV/K	l_g Å	U_g	E_f meV	$n \times 10^{20}$ cm^{-3}
320	6.41	87.10	6483×10^2	−0.0016	89.7	4.66
350	6.21	94.74	5782×10^2	−0.0016	90.3	4.81
400	6.00	96.31	4773×10^2	−0.002	101.4	4.87
450	5.72	88.96	3874×10^2	−0.0028	123.0	7.42
470	5.59	92.73	3453×10^2	−0.0022	124.0	7.69

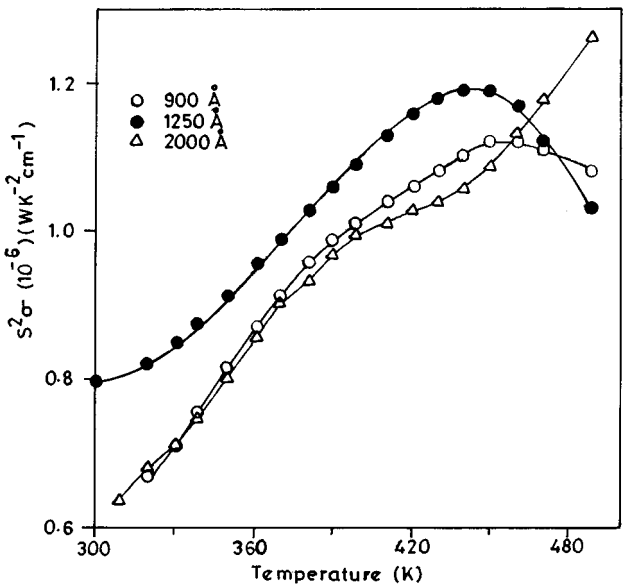

FIG. 8. $S^2\sigma$ as a function of temperature for different films.

ary scattering, the Seebeck coefficient of thin films as a function of thickness is given by the expression,

$$S_f = S_g\left[1 - \frac{3(1-p)l_g}{8t}\frac{U_g}{1+U_g}\right], \tag{5}$$

where

$$U_g = \frac{\partial \ln l_g}{\partial \ln E}. \tag{6}$$

S_g is the thermoelectric power of the hypothetical bulk given by the expression,

$$S_g = \frac{-\pi^2 k^2 T}{3eE_f}(1+U_g). \tag{7}$$

Figure 7 shows the plot of thermoelectric power versus $1000/t$ along with the straight line fit. The y intercept gives the value of S_g. From the slope of the straight line which is equal to $(3/8)l_g U_g/(1+U_g)$ the parameter U_g can be obtained using the l_g values obtained from the resistivity data analysis. The values of U_g and S_g thus calculated are tabulated in Table IV. It is found that U_g is temperature dependent and negative which indicates that the carrier mean-free path depends on its energy and decreases with energy. The Fermi energy values have been calculated from relation (7) at different temperatures using the calculated U_g values and are given in Table IV. It is found that the Fermi energy value and the electron concentration increase slightly with temperature. The carrier concentration was calculated using the following relation for partially degenerate semiconductors:

$$n = \frac{4\pi}{\pi^{1/2}}(2\pi m^* kT/h^2)^{3/2}F_{1/2}, \tag{8}$$

where m^* is the effective mass of the charge carriers, T the temperature, and $F_{1/2}$ the Fermi integral. The carrier concentration was calculated using the reported value[22] of $m^*/m = 1.068$.

Lidorenko *et al.*[38] have determined the electron concentration using the measured Hall coefficient which is of the order of 10^{20} cm^{-3} for this material. Our results agree with this. The sudden increase of the electron concentration around 450 K (see Table IV) is attributed to the creation of charge carriers due to the formation of structural defects. These, as explained earlier, are the result of oxygen desorption from the films.

The thermoelectric power factor $S^2\sigma$ was calculated at different temperatures from the measured thermoelectric power and electrical resistivity values. Plots of $S^2\sigma$ versus temperature for different film thicknesses are shown in Fig. 8. It is seen that the thermoelectric power factor increases linearly in the low temperature range and then tends to bend towards the temperature axis, which is similar to the thermoelectric behavior of the films. But the thermoelectric power factor value is low compared to the reported bulk thermoelectric power factor value. This is expected given the high resistivity of thin films.

IV. CONCLUSIONS

Thin films prepared by the flash evaporation technique are stoichiometric in composition. The grain size of the films increases with thickness. The thickness dependence of thermal activation energy is explained by Seto's grain boundary trap model. The decrease of thermoelectric power in the high temperature region is explained to be due to the partial evaporation of Te atoms and the occupation of Te sites by Bi/Se atoms. The thickness dependences of thermoelectric power and resistivity are explained by the classical size effect theory. Further, various important physical parameters are evaluated. The low values of the thermoelectric power factor of the films are due to the high resistance of the films.

ACKNOWLEDGMENTS

One of the authors (S.S.) is thankful to Indian Institute of Technology, Madras (India) for financial assistance. The authors are thankful to D. Kanchana Mala, Metallurgical Department for her help in TEM and EDAX measurements.

[1] A. F. Ioffe, *Semiconductor Thermoelements and Thermoelectric Cooling* (Infosearch, London, 1957).
[2] S. Misra and M. B. Bever, J. Phys. Chem. Solids **25**, 1233 (1964).
[3] S. Nakajima, J. Phys. Chem. Solids **24**, 479 (1963).
[4] J. A. Bland and S. J. Basinski, Can. J. Phys. **39**, 1040 (1961).
[5] J. R. Wiese and L. Muldawer, J. Phys. Chem. Solids **15**, 13 (1960).
[6] C. H. Champness, P. T. Chang, K. Grabowski, and W. B. Muir, J. Appl. Phys. **39**, 4177 (1968).
[7] N. K. Stark, T. E. Svechnikova, and S. N. Chizhevskaya, Inorg. Mater. **21**, 328 (1985).
[8] V. F. Bankina and N. Kh. Abrikosov, Russ. J. Inorg. Chem. **9**, 509 (1964).
[9] E. Kh. Shokr, M. M. Wakkad, M. M. Abd El-Reheem, and N. M. Megahed, Indian J. Pure Appl. Phys. **33**, 323 (1995).
[10] Y. A. Arifov, A. I. Kulagin, N. I. Erzin, N. V. Makov, B. Tursunov, and H. Saidvalieva, Appl. Solar Energy **10**, 63 (1974).
[11] U. A. Arifov, N. I. Erzin, A. I. Kulagin, N. V. Makov, Z. M. Dashevskii, L. L Lukashevich, and Kh. Kh. Khafizov, Appl. Solar Energy **11**, 3 (1975).
[12] I.-H. Kim and D. H. Lee, *Fifteenth International Conference on Thermoelectrics Proceedings, ICT 1996* (IEEE, New York, 1996), pp. 425–429.
[13] L.-H. Kim and D.-H. Lee, J. Mater. Res. **12**, 423 (1997).
[14] I.-H. Kim and D.-H. Lee, Korean J. Mater. Res. **6**, 121 (1996).
[15] A. V. Wagner, R. J. Foreman, L. J. Summers, T. W. Barbee, and J. C.

Farmer, *Fourteenth International Conference on Thermoelectrics Proceedings*, edited by M. V. Vedernikov, M. I. Fedorov, and A. E. Kaliazin (A. F. Ioffe Institute of Physics, St. Petersburg, Russia), 1995, pp. 283–287.
[16] A. V. Wagner, R. J. Foreman, L. J. Summers, T. W. Barbee, and J. C. Farmer, in *Fifteenth International Conference on Thermoelectrics Proceedings, ICT 1996* (IEEE, New York, 1996), pp. 269–273.
[17] A. V. Wagner, R. J. Foreman, T. W. Barbee, and J. C. Farmer, in *Fifteenth International Conference on Thermoelectrics Proceedings, ICT 1996* (IEEE, New York, 1996), pp. 459–463.
[18] A. V. Wagner, R. J. Foreman, L. J. Summers, T. W. Barbee, and J. C. Farmer, in *Proceedings of the 30th Intersociety Energy Conversion Engineering Conference*, edited by D. Yooi Goswami, L. D. Kannberg, T. R. Mancini, and S. Somasundaram (ASME, New York, 1995), Vol. 3, p. 87.
[19] J. C. Farmer, T. W. Barbee, G. C. Chapline, Jr., R. J. Foreman, L. J. Summers, M. S. Dresselhaus, and L. D. Hicks, in *Thirteenth International Conference on Thermoelectrics*, American Institute of Physics Conference Proceedings, Iss No. 316 (AIP, New York, 1995), pp. 217–225.
[20] J. C. Farmer, T. W. Barbee, R. J. Foreman, and L. J. Summers, in *185th Electrochem. Society Meeting, San Francisco, CA, 22–27 May 1994* (Electrochem. Soc., Pennington, NJ, 1994), pp. 231–242.
[21] J. C. Farmer, S. Ghamaty, and B. Elsner, Symposium on Materials Synthesis and Characterization, 207th Meeting of the American Chemical Society, San Diego, CA, 13–17 March 1994 (unpublished), Paper No. 74.
[22] J. C. Farmer, T. W. Barbee, R. J. Foreman, and L. J. Summers, in *185th Electrochem. Soc. Meeting, San Francisco, CA*, 22–27 May 1994 (Electrochem. Soc., Pennington, NJ, 1994), pp. 1661–62.
[23] J. P. McHugh and W. A. Tiller, Trans AIME **215**, 651 (1959).
[24] V. Damodara Das and P. Gopal Ganesan, *National Conference on Developments in Electronic Materials and Their Applications* (Shivaji University, Kolhapur, India, 1995).
[25] B. D. Cullity, in *Elements of X-ray Diffraction*, 2nd ed. (Addison-Wesley, Reading, MA, 1978), p. 284.
[26] J. Y. W. Seto, J. Appl. Phys. **46**, 5247 (1975).
[27] V. Damodara Das and P. Gopal Ganesan, Semicond. Sci. Technol. **12**, 195 (1997).
[28] V. Damodara Das and C. Bahulayan, Solid State Commun. **93**, 949 (1995).
[29] I. Teramoto and S. Takayanaki, J. Phys. Chem. Solids **19**, 124 (1961).
[30] A. F. Joffe and L. S. Stil'bans, Rep. Prog. Phys. **XXII**, 167 (1959).
[31] E. H. Sondheimer, Adv. Phys. **1**, 1 (1952).
[32] M. S. P. Lucas, Appl. Phys. Lett. **4**, 73 (1964).
[33] A. A. Cottey, Thin Solid Films **1**, 297 (1968).
[34] J. E. Parrot, Proc. Phys. Soc. London **85**, 1143 (1965).
[35] A. F. Mayadas and M. Shatzkes, Phys. Rev. B **1**, 1382 (1970).
[36] C. R. Tellier, Thin Solid Films **51**, 311 (1978).
[37] C. R. Pichard, C. R. Tellier, and A. J. Tosser, J. Phys. F **10**, 2009 (1980).
[38] N. S. Lidorenko, Z. N. Dashevskii, T. M. Erusalimskaya, Ya. A. Kaller, and N. V. Kolomoets, Sov. Phys. Dokl. **24**, 286 (1979).